Deep Dielectric Charging Of Spacecraft Polymers by Energetic Protons

Nelson W. Green and JR Dennison

***Abstract*— The majority of research in the field of spacecraft charging concentrates on electron charging effects with little discussion of charging by protons. For spacecraft orbiting in the traditional LEO and GEO environments, this emphasis on electrons is appropriate since energetic electrons are the dominant species. But for spacecraft in orbits within the inner radiation belts, or for interplanetary and lunar space probes, proton charging effects may also be of concern. To examine bulk spacecraft charging effects in these environments several typical highly insulating spacecraft polymers were exposed to energetic protons with energies from 1 MeV to 10 MeV to simulate protons from the solar wind and from solar energetic proton events. Results indicate that effects in proton-charged dielectrics are distinctly different than those observed due to electron charging. In most cases, the positive surface potential continued to increase for periods on the order of minutes to a day, followed by long time scale decay at rates similar to those observed for electron charging. All samples charged to positive potentials, with substantially lower magnitudes than for equivalent electron fluence. Possible explanations for the different behavior of the measured surface potentials from proton irradiation are discussed; these are related to the evolving internal charge distribution from energy dependent electron and proton transport, electron emission, charge migration due to dark current and radiation induced conductivity, and electron capture by embedded protons.**

***Index Terms*—Protons, electrons, charge storage, dielectric discharge, spacecraft charging, resistivity, conductivity, and radiation induced conductivity.**

I. Introduction

CHARGING of spacecraft through exposure to the space environment continues to be a topic of concern for spacecraft designers and operators. Collections of large quantities of charge on the surface of the spacecraft or in the bulk of dielectric materials on board can lead to electrostatic discharges (ESD) causing severe damage to spacecraft systems up to and including loss of the mission [1, 2]. Since a majority of spacecraft operate in the low earth and geosynchronous orbits where electron effects dominate, most spacecraft charging studies have centered on the collection of charge either through direct electron exposure, secondary electron effects, or through the photoelectric effect. Little research, however, has been performed on the charging effects of proton exposure on spacecraft surfaces or the collection of protons in the bulk of spacecraft dielectrics.

Since few, if any, examples of ESD have been reported due to fluxes of protons, the paucity of research into proton charging is understandable. There is, however, an increased desire to operate spacecraft in regions such as within the inner Van Allen belts, or in lunar operations, which represent space environments where energetic protons are more prevalent [3]. Long duration interplanetary missions also have the potential to be exposed to high fluxes of solar energetic particles during coronal mass ejections (CME).

This paper presents the results of recent experiments examining the ability of protons to produce ESD and the ability for typical spacecraft dielectrics to dissipate accumulated charge due to energetic proton exposure.

II. Experiments

While few researchers have conducted charging experiments with protons, there exist reports of visible discharges in glasses that support the capability of incident protons to induce sufficiently large electric fields to exceed the field strength of the material and cause dielectric breakdown. In the majority of the reported cases, highly energetic protons were implanted utilizing high current densities leading to large breakdowns and the formation of visible Lichtenberg figures [4-10]. While such discharges could be disastrous for a spacecraft, damage can be done to sensitive electronics with far smaller discharges. The high energies and large proton fluxes used in these previous studies are also rarely, if ever, found in the space environment, causing the applicability of such tests to be limited.

In order to determine more realistic testing conditions, a simple parallel plate capacitor model consisting of a pair of infinite sheets of opposing charges—representing, for example, a layer of charge deposition in an insulator and an image charge layer in a grounded conducting backplane—was used as a worst case example of a charged dielectric. The model further assumes negligible discharge during bombardment, meaning that the dark current decay time is much longer than the duration of charging. Using Gauss' law and the generalized breakdown field strength of 10^7 V/m

Manuscript received XXXX.

Nelson W. Green is a member of the engineering staff at the Jet Propulsion Laboratory, California Institute of Technology, 4800 Oak Grove Drive, Pasadena, CA 91109-8099, USA (Phone: 818-393-6323; fax: 818-393-0351; email: Nelson.W.Green@jpl.nasa.gov).

JR Dennison, is a professor with the Physics Department at Utah State University, Logan, UT 84321 USA (Phone: 435-797-2936; fax: 435-797-2492; e-mail: JR.Dennison@usu.edu).

applicable for most dielectric materials, the minimum fluence of charges required to induce a dielectric breakdown is on the order of 10^{10} charges/cm^2. This critical breakdown strength is the same order of magnitude for a wide array of insulating materials; it is approximately the electric field required for an elemental charge to obtain the ionization potential in one mean free path length (on order of 10 eV) for a low energy electron in an insulator (~1 μm). This calculation is polarity independent and receives some confirmation from the results of the Internal Discharge Monitor (IDM) on the Combined Release and Radiation Effects Satellite (CRRES). The first discharges reported for the various dielectrics in the IDM started occurred with electron fluences of approximately 2x10^{10} electrons/cm^2.

Using the calculated fluence of 10^{10} proton/cm^2 as the minimum required for dielectric breakdown, the JPL 1991 Solar Proton Model [11, 12] was consulted to determine likely energy ranges for testing. This model examines protons in several energy ranges as measured at 1 AU during Solar Energetic Proton events and CME's over three and a half solar cycles including the largest events seen to date. In all cases, fluences of 10^{10} protons/cm^2 were limited to energies of <30 MeV with only a few CMEs providing sufficient proton fluence at 10 MeV to produce a discharge.

A. Dielectric Discharge Testing

Based on these calculations, an experiment utilizing 10 MeV protons was conducted on nine representative dielectrics typically found on spacecraft. Samples chosen for the Prometheus materials test included four fluoropolymers (polytetrafluoroethylene (PTFE), fluorinated ethylene propylene (FEP), perfluoroalkoxy (PFA), and ethylene tetrafluoroethylene (ETFE)), three urethane-based potting compounds (Conathane, Uralane, and Solithane), RTV Silicone rubber, and a polyimide E-glass printed circuit board composite material (Arlon). This paper focuses on results for four representative dielectric materials:

The PTFE bulk polymer sample tested is a "Virgin Electrical Grade" polytetraflouroethylene material.

Arlon 85N is a composite printed circuit board material, using an E-glass cloth as a prepreg material. The resin used was a pure Kapton E polyamide resin. The material had a ~30 μm thick coating of Probimer 52 solder mask on the front surface.

Conathane EN-11is an opaque amber material.

Uralane 5750 (now called Arathane 5750 A) is an amber translucent material. Conathane and Uralane are both soft, ASTM Type 5 two-component, polybutadiene-based liquid urethane casting and potting compounds with polyol-cured resins used for potting and conformal coating and as a bonding agent.

Table 1 lists relevant sample characteristics and materials properties. Typical samples had a 25 cm^2 area, with thicknesses ranging from 1 to 3 mm. Each was equipped with a copper electrode on one face and mounted so that the other face would be directly exposed in vacuum one sample at a time to the incident energetic protons.

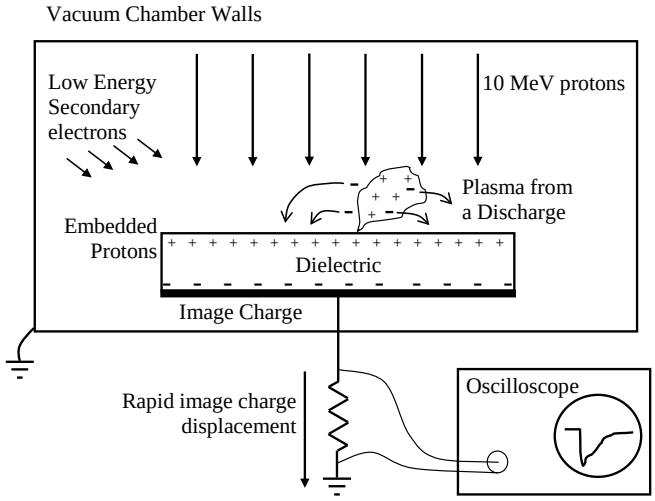

Figure 1. Schematic of instrumentation for measurement of dielectric discharge pulses during energetic proton bombardment experiments.

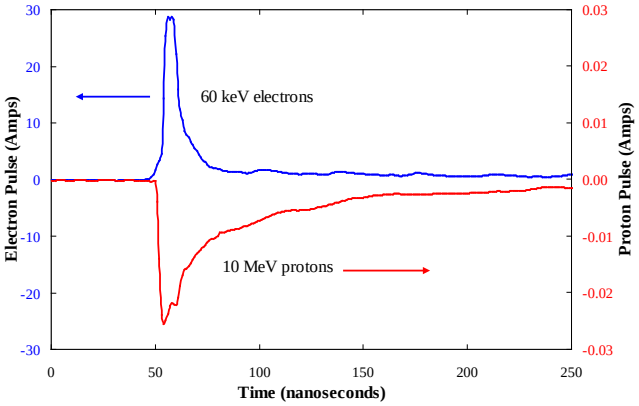

Figure 2. Comparison of dielectric current discharge pulse profiles from proton and electron exposure of Kapton E polyimide printed circuit board material.

High energy proton dielectric discharge testing was conducted at the University of California, Davis, using a cyclotron accelerator with a 10 MeV pulsed proton beam. Each of the samples materials, listed in Table 1, was exposed to the proton beam at current densities of 0.1 to 1 nA/cm^2 for times of up to several hours leading to fluences of 10^{12} to 10^{13} protons/cm^2. At these energies the protons penetrated the dielectric up to ~1 mm or between 20% and 50% of the sample thickness, depositing the full incident charge within the bulk of the material. The corresponding energy deposition density or total dose imparted to the sample was on the order of ~4·10^7 rad. Above 10^6 to 10^7 rad, significant permanent structural radiation damage can be expected in such polymeric materials, while permanent changes in the electronic structure are often evident above 10^5 to 10^6 rad. Typical dose rates were ~3·10^3 rad/sec. Above 10^{-1} to 10^1 rad/sec, radiation induced conductivity (RIC) can be expected to exceed dark current conductivities, leading to orders of magnitude increases in total conductivity; RIC is approximately linearly proportional to dose rate [17]. All exposures and measurements were conducted in a vacuum of ~10^{-5} torr at room temperature.

TABLE 1. PHYSICAL PROPERTIES OF SAMPLES

Characteristic	(Units)	Sample			
		PTFE	Kapton E-(Arlon-85N) [a]	Conathane (EN-11)	Uralane (5750)
Electrical and Materials Properties					
Density	(g/cm^3)	2.15	1.7	0.98	1.21
Thickness	(mm)	3.17	1.52 [a]	2.41	2.41
Relative Dielectric Constant	unitless	2.0 (1 MHz)	4.39 (1 MHz)	3.30 (100 Hz)	3.33 (100 Hz)
Electrostatic Breakdown Strength [b]	(MV/m) (kV)	~150 48	48 7.3	24 5.8	14 3.4
Electron Dark Current Resistivity [c,j]	(Ω-cm)	$6\cdot10^{19}$	$2\cdot10^{19}$	$5\cdot10^{17}$	$4\cdot10^{18}$
Electron Dark Current Decay Time [c,d,j]	(days)	137	80	1.7	14
Electron Yields and Penetration Depths					
Max. Electron Yield (@~1 keV) [e]	(elec/elec)	~4	~3	~3	~3
Electron Yield (45 keV electrons) [e]	(elec/elec)	~0.3	~0.2	~0.2	~0.2
Electron Yield (1 MeV protons) [e,f]	(elec/proton)	3-4	3-4	3-4	3-4
Electron Yield (10 MeV protons) [e,f]	(elec/proton)	2-3	2-3	2-3	2-3
Range (45 keV electrons) [g]	(μm)	20	23	36	29
Range (10 MeV protons) [g]	(μm)	717	793	1230	996
Range (1 MeV protons) [g,h]	(μm)	15	16	24	19
Characterization of RIC and Radiation Damage					
Penetration (1 MeV protons) [g,h]	(% of thickness)	0.5	1.0	1.0	0.8
Total Dose [g,h]	(Mrad)	55	66	78	78
Dose Rate [g,h]	(rad/s)	$9\cdot10^{4}$	$1\cdot10^{5}$	$1\cdot10^{5}$	$1\cdot10^{5}$
RIC Resistivity [g,h,i]	(Ω-cm)	$2\cdot10^{12}$	$2\cdot10^{11}$	$2\cdot10^{11}$	$2\cdot10^{11}$
RIC Decay Time [d,g,,h,i]	(min)	20	14	14	14
Proton Dark Current Resistivity [h,j]	(Ω-cm)	(no decay observed)	$2\cdot10^{19}$	$8\cdot10^{17}$	$6\cdot10^{18}$
Proton Dark Current Decay Time [h,d]	(days)	(no decay observed)	89	2.8	19

[a] Kapton E-glass composite circuit board material with ~3 μm thick layer of Probimer 52 mask material on vacuum side surface.
[b] Manufacturer's values at room temperature and ~30% RH.
[c] Measured by charge storage method with 45 keV incident electrons [13].
[d] Calculated as product of resistivity, dielectric constant, and permittivity of free space.
[e] Measured values at normal incidence [14]. Kapton E, Conathane and Uralane assumed similar to Kapton HN values.
[f] Estimations based on values for graphitic carbon at normal incidence [15].
[g] Based on values in [16].
[h] Based on values for 1 MeV incident protons.
[i] Measured values; see [17]. Conathane and Uralane assumed similar to Kapton E values.
[j] Using long-time decay constant method [18].

Each sample was monitored for discharges using an oscilloscope connected between the sample's rear electrode and ground, as illustrated in Figure 1. As protons were implanted within the sample material, negative charges were transferred from the ground reservoir to oppose the implanted protons, slowly forming a layer of image charge at the interface between the dielectric and the copper electrode.

During a discharge, the rapid depletion of charge in the dielectric produced a mirror movement of image charge from the rear electrode. The rapid movement to ground of the collected image charge was recorded as a current pulse by an oscilloscope connected across a 50 Ω current limiting resistor in series with the sample.

Dielectric discharges were recorded during proton exposure, but only on the polyimide material. The pulses that were captured were few in number and typically three orders of magnitude smaller current than those produced by comparable electron exposure. While the sign of electron and proton pulses were opposite as expected, the general shapes and durations of the pulses were similar as seen in Figure 2.

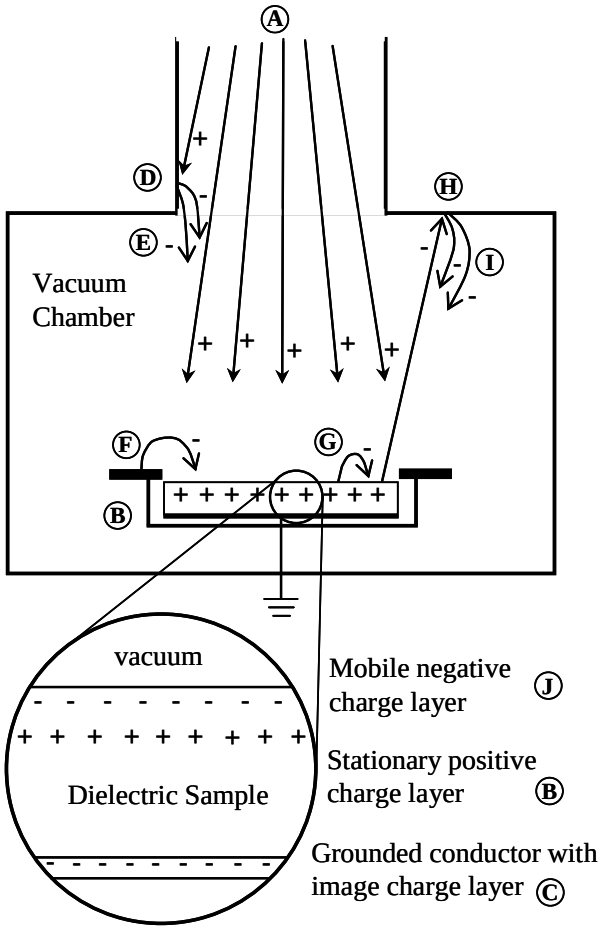

Figure 3. Schematic diagram of the proton charging experiment. A 1 MeV proton beam (A) is incident on a dielectric sample of thickness *D*. Deposited protons form a stationary positive charge layer (B) at a depth *R* below the surface of the dielectric. A negative image charge layer (C) is formed in the grounded conducting backplane. Electrons from this charge layer slowly migrate toward the fixed positive charge layer with a time constant τ_{DC} proportional to the dark current resistivity. Stray high energy protons from the uncollimated beam (D) collide with the chamber walls, producing secondary electron (E). Protons (A) incident on the sample shields also produce secondary electron (F). Incident protons (A) also produce low energy secondary electrons (G) and higher energy backscattered electron (H) [which in turn produce low energy electrons (I) in collisions with the grounded chamber walls]. These secondary electrons, (E) (F) (G) and (I), are attracted to the positively biased surface of the dielectric and form a mobile negative charge layer (J) at a depth *d* below the surface that migrates more rapidly toward the fixed positive charge layer with a time constant τ_{RIC} proportional to the sample dose rate. (τ_{RIC} is time-dependant after the proton beam is turned off. Diagrams are not to scale.

This similarity suggests that the same conduction mechanisms might be responsible for both electron and proton discharges, while the amplitude of charge transfer was much less for proton bombardment.

1) Charge storage testing

In addition to electrostatic discharge testing, the selected dielectrics were tested for charge storage properties when exposed to 1 MeV protons; in a separate experiment these same materials were also tested with 45 keV electrons [14, 17]. The electron and proton energies were selected to allow comparable charge particle penetration and deposition of the full incident charge within the sample. Independent tests using both protons and electrons were utilized to give a direct comparison for the response of the materials to both types of particles. Figure 3 shows a schematic of the experimental apparatus for proton bombardment experiments. A similar set up was used for the electron bombardment experiments [19].

Figure 4 shows surface potentials as a function of elapsed time as a result of bombardment with 45 keV electrons and 1 MeV protons for the same samples detailed in the dielectric discharge testing. Characteristics of the voltage decay curves are listed in Table 1. It is interesting to contrast the basic features exhibited by these two sets of surface potential plots:

a) Electron Bombardment

Electron bombardment charge storage testing was conducted in a dedicated high vacuum chamber at the Jet Propulsion Laboratory using a continuous beam electron flood gun [19]. Samples were exposed to current densities of 4 nA/cm^2 at 45 keV incident energy for times up to several minutes, leading to fluences of ~10^{12} electrons/cm^2. At these energies, the electrons penetrated up to ~25 μm or 0.5% to 2% of the sample thickness (see Table 1). The corresponding energy deposition density was a total dose of 10^5 rad, which is likely to cause significant permanent electrical radiation damage. Typical dose rates were 10^3 rad/sec; at these high dose rates RIC can be expected to exceed dark current conductivities by 4 to 6 orders of magnitude.

The materials all charged to *negative* surface potentials on the order of ~10^3 V. Each curve exhibited a rapid decrease in surface potential occurring on a time scale of 10^3 to 10^4 sec, attributed to polarization of the material. At longer times, on the order of days, the materials exhibit approximately exponential voltage decay [19, 20], with time constants (dark current decay times) of from 1.7 to 137 days. The decay time constant, τ_{DC}, was related to the dark current resistivity, ρ_{DC}, in the parallel plate capacitor approximation as $\tau_{DC}=\rho_{DC}\varepsilon_o\varepsilon_r$, where ε_o is the permittivity of free space and ε_r is the relative dielectric constant. The general nature of these voltage curves has been largely explained by a simple macroscopic model in terms of the dielectric constant, polarization time and dark current resistivity [13, 19].

b) Proton Bombardment

Proton bombardment charge storage testing was conducted in a dedicated high vacuum chamber at the United States Air Force Academy using an accelerator that produced a continuous proton beam. The small beam area (~1 cm^2) was rastered across a rectangular area at a repetition rate of ~0.3 msec, spending ~¾±¼ of the time incident on the 25 cm^2 sample and the rest of the time incident on grounded stainless steel or aluminum shielding. Samples were exposed to average current densities of ~3 nA/cm^2 at 1 MeV incident energy for 10 min, leading to fluences of ~10^{13} protons/cm^2. At these energies, the protons penetrated up to 20 μm or 0.5% to 1% of the sample thickness (see Table 1). The corresponding energy deposition density was a total dose of 10^7 rad, which is likely to cause significant permanent structural radiation damage. Typical dose rates were 10^5 rad/sec; at these high dose rates

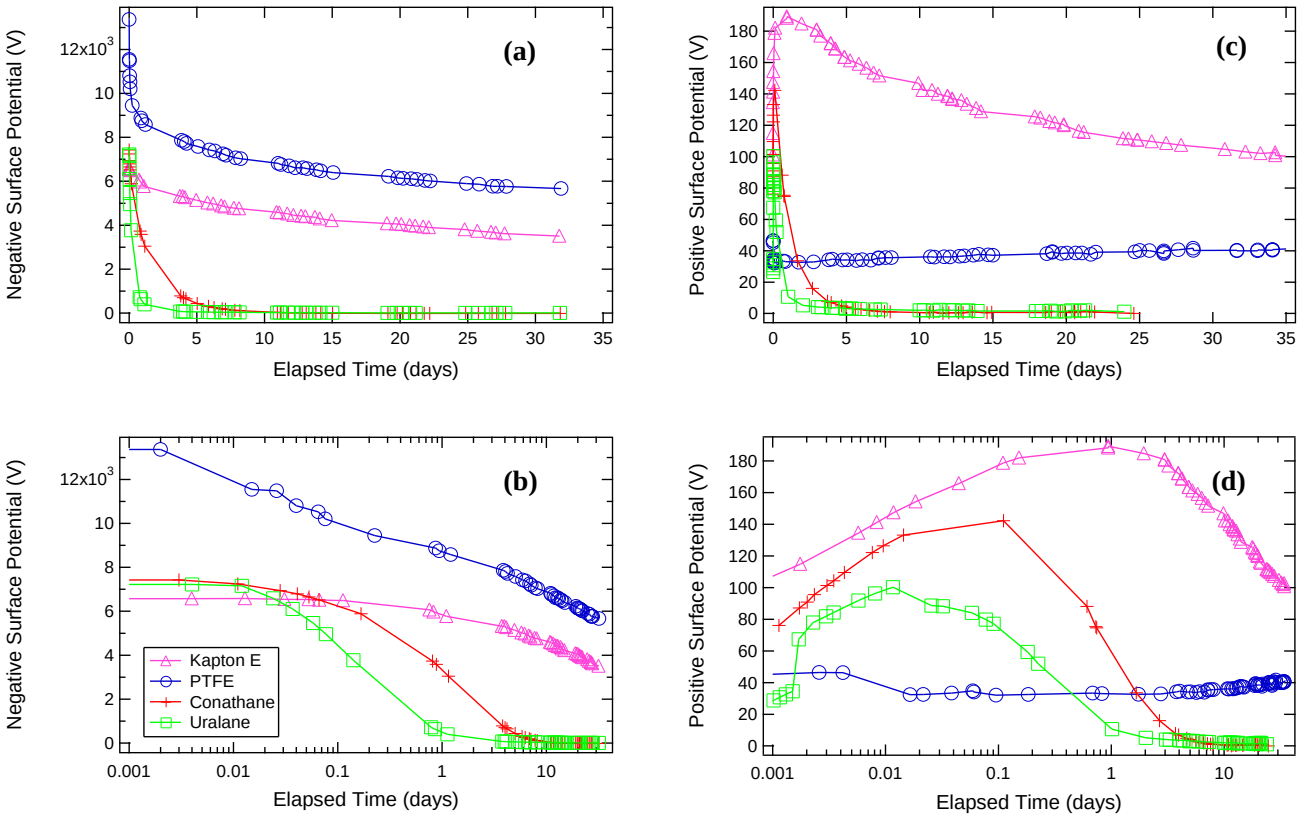

Figure 4. Surface potentials as a function of elapsed time for (a-b) 45 keV electron and (c-d) 1 MeV proton charged dielectrics. Note that (a) and (c) are linear plots while (b) and (d) have logarithmic time axes.

RIC can be expected to exceed dark current conductivities by 4 to 6 orders of magnitude.

After exposure, the materials all charged to *positive* surface potentials to ~10^2 V. Despite a proton fluence of approximately 4 times the electron fluence, the magnitudes of the measured surface potentials were only 0.3% to 2% those measured for electron bombardment. Each of the materials (except PTFE whose behavior is not consistent and could not be analyzed using similar models since its surface potential did not decay with time) showed a similar trend in their surface voltage versus elapsed time curves. Each exhibited an *increase* in surface potential, to approximately twice that of the initial measurement taken ~1 min after the proton beam was shut off. The increases occurred over time scales from ~15 min for Uralane to ~1 day for the Kapton E composite. After this initial increase, the three materials all had monotonic decreases in surface voltage. At long time scales, the materials again exhibited approximately exponential voltage decay, with time constants (dark current decay times) of from 2.8 to 89 days (see Table 1). The decay constants found for the proton bombardment were somewhat smaller than those found for electron bombardment, but agreed within a factor of two for each of the three materials.

III. DISCUSSION OF RESULTS

A successful model of the behavior of these materials during and after the proton bombardment experiments must, at least qualitatively, predict the following five different observed trends:

(i)The surface potential is positive after bombardment, in contrast to negative potentials for electron bombardment.

(ii) The number and amplitude of observed electrostatic discharges is much lower than predicted based solely on the incident charge density.

(iii) The magnitudes of the proton bombardment surface potentials were much less than for electron bombardment. The potential magnitudes were only ~1% of those observed for electron bombardment; the potential magnitudes per fluence for proton bombardment were a factor of 10^2 to 10^3 less than for electron bombardment.

(iv) The surface potentials initially increased with time, reaching approximately twice the initial measurements, over material-dependent time scales ranging from ~15 min to ~1 day.

(v) On a longer time scale, the voltage decayed approximately exponentially with time constants ranging from 2 to ~100 days. These dark current decay times were similar—to within a factor of two—of the dark current decay times observed for electron bombardment experiments.

A. Charge Distribution Model

As an explanation for this behavior, consider the following very simplified model for the time evolution of charge distribution within the samples during and after proton bombardment. The one dimensional model, shown in Figure

5, assumes all charge distributions are infinite sheets of negligible thickness. The material has a grounded conducting plane at $x= 0$, a fixed positive charge layer at $x=D-R$, a mobile negative charge layer at $x(t)=D-d(t)$; has a dielectric constant $\varepsilon_o\varepsilon_r$ and dark current resistivity ρ_{DC} and extends from $0<x<D$. Each charge layer, of charge density $\Sigma_{\pm}$, produces a uniform electric field of magnitude $E_{\pm}=\Sigma_{\pm}/2\varepsilon_0\varepsilon_r$, as shown. The samples are surrounded by a vacuum chamber with grounded conducting walls at a relatively large distance from the sample surface, as compared to the sample thickness. This model is similar to other multilayer charged models developed for similar purposes, such as the Double Dynamic Layer Model (DDLM) [21-24] and provides a reasonable approximation to the "highly nonuniform" multilayer charge distribution previously measured in similar Teflon films under 0.8 MeV proton irradiation [8].

Setting the potential at ground to zero volts, it follows that the surface potential after the beam is turned off, as a function of the distance of the mobile negative charge layer below the surface, d(t), is

$$V(t)=\left\{\left(D/2\varepsilon_0\varepsilon_r\right)\left[\Sigma_+\left(1-2R/D\right)-\Sigma_-\left(1-2d(t)/D\right)\right]\right\}\exp(-t/\varepsilon_o\varepsilon_r\rho_{DC}). \quad (1)$$

Measured values of $V(t)$ over long time scales are plotted in Figure 4 and during the initial voltage rise in Figure 6. We first consider the short term voltage rise, which is modeled by the initial term in curly brackets in Eq. (1), assuming that the rise occurs in a time that is short compared to the dark current decay time. If we assume an initial potential, V_o, and a maximum potential, V_{max}, at time $t_{max}\ll\tau_{DC}$ the charge densities follow as

$$\Sigma_- = \varepsilon_o\varepsilon_r\frac{(V_{\max}-V_o)}{R} \quad \text{and} \quad \Sigma_+ = \varepsilon_o\varepsilon_r\frac{(V_{\max}D-V_o(D-2R))}{R(D-2R)}. \quad (2)$$

The initial time dependence is then fully contained in the last term in the curly brackets, $2\Sigma_- d(t)/\varepsilon_o\varepsilon_r$. The model can be readily generalized to more complex charge evolutions by considering a modification of either the charge concentration or charge position. Σ_- can more generally represent the centroid of a charge distribution that can even have a time dependent magnitude. Physical limits require that Σ_- cannot increase in magnitude with time (since no new net charge is added when the beam is off), but could decrease due to recombination with protons as long as $\Sigma_+ + \Sigma_-$ is conserved. Further, $d(t)$ is not expected to decrease with time, since the negative charge layer is not expected to move away from the fixed positive charge layer and towards the incident proton beam (*e.g.*, move to the right in Figure 5).

1) 3.1.1 - Charge Deposition Period

We now consider the physical origins of the time evolution of the charge distribution and surface voltage, beginning with an uncharged sample when the proton beam is turned on. The incident protons penetrate a distance R into the sample and deposit charge. The sign of the surface potential is explained readily with Gauss' law by the sign of the deposited

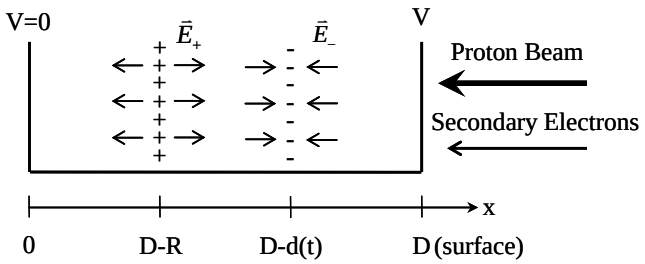

Figure 5. Simple charge slab model of charge within the sample. Shown are the grounded conducting plane at x= 0, the fixed positive charge layer at x=D-R, the mobile negative charge layer at x=D-d(t), and the dielectric surface at x=D. Also shown are the uniform electric fields from the charge layers. Diagram is not to scale.

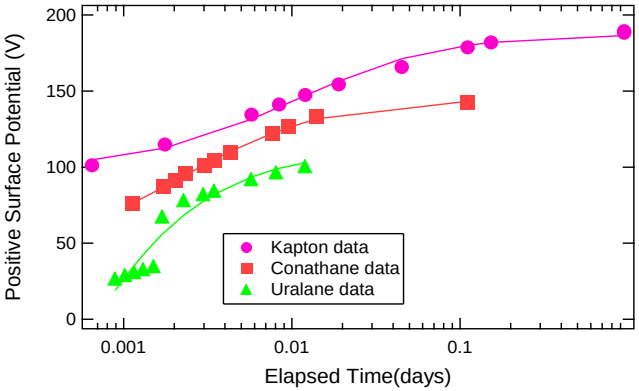

Figure 6. Surface potentials during the initial voltage rise as a function of elapsed time for 1 MeV proton charged dielectrics. The fit is based on Eq. (3), with the parameters listed in Table 2. Note the logarithmic time axes.

charge, positive for proton bombardment and negative for electron bombardment. The penetration depth of the charged particles is predicted to first order by Bethe theory [25, 26] to be at a narrow range, consistent with the notion of charge confined to a well defined charge layer. In the continuous slow down approximation (CSDA) energy is assumed to be deposited at a uniform rate up to the range R where all charge is assumed to be deposited. Values for R in the CSDA have been tabulated for common materials [16], as listed in Table 1. The range for both 45 keV electrons and 1 MeV protons is on the order of 25 μm or about 0.5-1.5% of the sample thickness.

However, deposition of the incident charge alone then predicts that the magnitude of the surface voltage is directly proportional to charge fluence with concomitant large magnitude potentials for the proton experiments. Based solely on the total proton charge deposited, ~2μC/cm^2, the predicted surface voltage is ~50 kV, far in excess of the electrostatic breakdown strength of the materials. The relatively few electrostatic discharges observed suggest that such high charge densities are never achieved. To maintain the three to four orders of magnitude lower surface voltages observed, we must have a lower *net* positive charge on the sample. Since the surface potential remains much lower than the kinetic energy of the incident protons, proton trajectories will not be significantly altered and essentially all protons in the beam should enter the sample. One possibility is for only a fraction of the incident protons to be trapped in the sample. Given the relatively large penetration depth of the high energy protons,

and their very low mobility once thermalized within the sample, this seems unlikely. Alternately, the incident protons could sputter positive ions from the surface of the sample. While some sputtering undoubtedly occurs, it should be negligible since only a small fraction of the incident proton's energy is deposited within a mean free path of a sputtered ion from the surface. Rather, it should be assumed that the incident protons are deposited in a charge plane at a depth equal to the CSDA range and remain fixed in position throughout the course of the ~1 month experiments. The vacancies in the relatively open polymer structure can readily accommodate the ~0.1 nanomole of hydrogen ions deposited during the duration of the proton bombardment. The number of deposited protons as neutralized H atoms occupies a gas volume at standard temperature and pressure of only 0.1 ppm of the irradiated volume of the sample (beam area times the proton range). Note that this upper limit of concentration of H atoms is only $\sim 10^{-7}$ that of possible H binding sites to the polymer chains in the irradiated volume; this suggests that chemical effects due to hydrogenation of the polymer are not likely to have a significant effect.

To achieve a lower net positive charge consistent with the lower observed surface potentials, we must then incorporate negative charges into the material during the course of the proton bombardment. As the initial protons are trapped within the material, the surface of the material will become positively biased and hence will attract free electrons. We consider four specific possible sources of these free electrons below. To maintain charge neutrality within the chamber (except on the sample), these free electrons must originate from conductors in contact with a grounded reservoir.

Incident protons will produce secondary electrons by emission from the sample surface. The number of ion-induced electron yields for 1 MeV protons at normal incidence is estimated to be ~3 to 4 electrons/proton for the polymeric materials under study. This estimate is based on measured values for graphitic carbon, since to first order, ion yield is proportional to mean atomic number [15]. Almost all of these proton-generated electrons will be low energy secondaries that will be immediately re-attracted to the positively biased surface [13]. This mechanism thus produces negligible *net* negative charge on the sample.

The relatively few ion-induced secondaries emitted from the sample with energies greater than the surface voltage can interact with the grounded chamber walls, producing additional low energy electrons. Electrons generated from interactions with the apparatus will also be attracted to the positively biased sample. Since the backscatter yield is small (except perhaps at grazing incidence) and the total yield is >1 for only a narrow range of incident energies between the crossover energies, this does not seem very likely as the source of enough electrons to neutralize almost all of the incident proton fluence. (Stainless steel has a backscatter yield of ~0.3 electrons/electron at normal incidence over a range of ~1 keV to 50 keV [14].)

Stray high energy protons can produce significant numbers of low to moderate energy electrons through interactions with the chamber walls or other grounded conducting surfaces. For example, protons from an uncollimated beam could interact with the chamber walls, often at grazing angles. The electron yields for Al and stainless steel are ~3-4 [15] for normal incident 1 MeV protons, and may be much higher for grazing angles (>50 electrons for angle >45°). The collection efficiency of these electrons by the surface would be quite high—even produced far from the sample surface—since the sample presumably is the only positively biased surface within the chamber. Therefore, if <2% of the protons in the beam interacted in such a way, this could produce more secondary electrons than in the total proton fluence.

Perhaps a more plausible source of ion-generated secondary electrons could be from the rastered proton beam hitting the Al and stainless steel grounded shields adjacent to the sample at normal incidence. Further, these secondary electrons would be produced in close proximity to the positively biased sample. Given the normal yield for 1 MeV protons, the rastered beam would have to only spend <25% of the time incident on the shielding to produce more secondary electron than in the total proton fluence.

TABLE 2. CHARACTERIZATION OF THE PROTON-INDUCED SURFACE VOLTAGE CURVES

Characteristic	(Units)	Sample			
		PTFE	Kapton E-(Arlon-85N) [a]	Conathane (EN-11)	Uralane (5750)
Measured First voltage	(V)	45	101	76	27
Elapsed time at first measured voltage	(sec)	73	56	98	77
Measured peak Voltage	(V)	46	189	142	100
Elapsed time at measured peak voltage	(sec)	223	81,712	9588	1006
Fit first voltage [a]	(V)	--	104 (103%)	76 (100%)	19 (69%)
Fit peak voltage [a]	(V)	--	187 (99%)	145 (102%)	112 (112%)
Fit RIC decay time [a]	(min)	--	14 (73%)	3.1 (21%)	0.5 (3%)
Initial positive charge layer density	(nC/cm^2)	0.17	21.1	8.0	9.1
Initial negative charge layer density	(nC/cm^2)	0.12	20.2	7.7	8.9

[a] Values in parentheses are ratios of fit to measured values.

It is central for the model to work that these free electrons attracted to the surface can readily recombine with the implanted protons. Due to the high dose rate experienced in the region between the surface and the positive charge layer during proton bombardment, RIC can be expected to greatly increase the mobility of the attracted electrons through this region. Values listed in Table 1 show that conductivities are enhanced by a factor of ~10^6 assuming RIC is linearly proportional to dose rate [17, 21, 22]. This model predicts charge transport decay times on the order of 10^{-1} seconds. Note that the calculated magnitudes of Σ_+ and Σ_- based on Eq. (2), listed in Table 2, are only ~10^{-3} times that of the total proton fluence, which suggests that most of the protons have recombined prior to when the beam was turned off. In fact, this decay time is on the order of 10^{-4} times that of the bombardment duration, which is in reasonable agreement with the estimate of the fraction of the charge in Σ_+ remaining when the beam was turned off. It should also be noted that the initial surface potentials of ~25 eV to 100 eV, listed in Table 2, are close to the first crossover energies of electron-induced yields on typical insulators [13]. It is expected that as the surface charges from proton fluence, it will reach an equilibrium surface potential equal to the difference between the first crossover energy and the secondary electron incident energy [21, 22, 24, 27]; at this equilibrium potential the yield is one and additional excess fluence will no longer be attracted to the surface [28]. Alternatively, Boyev et. al propose that the equilibrium surface potential achieved during proton irradiation is directly proportional to the ratio of the incident proton current to the RIC conductivity [10]; this predicts surface potential values of 1 V to 10 V for the studies here based on RIC conductivities at average dose rates and higher potentials as the RIC conductivity diminishes with time.

2) Post-Deposition Charge Migration Period of Voltage Increase

Immediately after the removal of the beam, there exist three layers of charge and two separate regions in the dielectric sample. The layers of charge are the un-neutralized implanted protons from the energetic proton beam, image charges from ground on the rear electrode, and residual attracted secondary electrons near the surface. The regions in the dielectric are the region of increased conduction due to RIC between the sample surface and the protons and the unirradiated bulk of the sample between the positive charge and grounded rear electrode.

The increased conductivity in the forward region allows electrons in the negative charge layer to migrate toward the fixed positively charged proton layer. As they move towards the grounded electrode, the effective negative surface potential decreases making the surface potential of the sample more positive over a short period of time. The increase in positive potential is limited by the temporary duration of the RIC and the distance the electrons must travel to reach the positive charge layer. As the effective conductivity of the material diminishes and the electrons that could move reach the positive charges, the increase in surface potential will halt. One important observed property of RIC is that this effect persists after the beam is extinguished; σ_{RIC} decreases inversely proportional to the elapsed time after the beam is turned off, that is $\sigma_{RIC}(t)=\sigma_{RICo}(1+t/\tau_{RIC})^{-1}$ with τ_{RIC} as the hyperbolic RIC time constant. [17,29]. Therefore, the motion of the negative charge layer towards the fixed positive layer slows with increasing time. Figure 6 shows a fit to the surface potentials of three materials during the initial voltage rise as a function of elapsed time based on the time-dependent model of surface voltage

$$V(t) = V_{\max} + (V_o - V_{\max}) \cdot (1 + t/\tau_{RIC})^{-1} \qquad (3)$$

where, from Eq. (2), the initial and final voltages can be related to the charge distributions and geometry of the DDLM as

$$V_o = \frac{1}{\varepsilon_o \varepsilon_r}\left[\Sigma_+\left(\frac{D}{2} - R\right) - \Sigma_-\left(\frac{D}{2}\right)\right] \qquad (3a)$$

$$V_{\max} - V_o = \frac{1}{\varepsilon_o \varepsilon_r}\Sigma_- R$$

The values of V_o and V_{max} plus $\tau_{RIC}$for the three materials determined from least squares fits shown in Fig. 6 are listed in Table 2. The fits based on Eq. (3) are quite good; the voltage parameters are on average within <10% of measured values, while τ_{RIC} is a factor of 3 to 30 lower than the approximate values measured by independent RIC tests [17] provided in Table 1.

3) Long Term Charge Dissipation Period

Once the electrons in the negative charge layer have reached the positive charge layer and recombined with the protons (or effectively stalled as RIC conductivity returns to negligible values), the time evolution of the voltage is driven by the dark current resistivity of electrons migrating from the grounded electrode to the fixed positive charge layer. This is modeled by the final exponential term in Eq. (1). In all samples except the Teflon materials, the calculated resistivity for the long time scale decrease in surface voltage is very nearly that found during electron-based charge storage experiments. These results lead to the conclusion that over long time for both electron and proton charged dielectrics the mechanism for charge migration through the material is comparable.

IV. CONCLUSION

Proton based spacecraft charging has been little studied due to a dearth of spacecraft operating in regions rich in energetic protons and a general assumption that they are of little danger to spacecraft. With an increased interest in operating in regions containing energetic protons, both in Earth orbit and in interplanetary missions, an examination of proton charging is relevant.

Two experiments were conducted to examine the responses of four typical polymeric dielectric materials to energetic proton bombardment. Results indicate that effects in proton charged dielectrics are distinctly different than those observed due to electron charging. A simple, two layer charge model was developed that explained the distinct, complicated behavior of the time evolution of the surface charge during and after proton bombardment. The explanation evolves internal charge distribution from energy dependent electron and proton transport, electron emission, charge migration due to dark current and radiation induced conductivity, and electron capture by embedded protons. Results showed that while dielectric discharges may occur during proton bombardment, they are quite small and few in number when compared with electron bombardment. Examination of the ability of the sample materials to store charge from implanted protons suggests that the increased conductivity of the material due to proton bombardment (RIC) allowed residual secondary electrons attracted to the positively biased sample surface to neutralize a majority of the implanted protons concurrent with bombardment, leading to relatively small net electric fields within the bulk of the dielectric. In most cases, the positive surface potential continued to increase after the proton beam was turned off, for periods on the order of minutes to a day. Both the amplitude and the unusual time evolution of the voltage are consistent with the hyperbolic reduction of persistent RIC that scales as 1/t. This voltage increase was followed by long time scale decay at rates similar to those observed for electron charging, suggesting that electrons dominate as the mobile particle in the bulk of both proton and electron charged dielectrics.

ACKNOWLEDGEMENTS

The measurements described in this paper were carried out at the Jet Propulsion Laboratory, the California Institute of Technology under a contract with the National Aeronautics and Space Administration. The authors gratefully acknowledge the following colleagues for their contributions of data and expertise: A. Shapiro, P. Willis, H. Garrett, D. Brinza, C. Benson, H. Kirkham, M. Petkov, and P. Bowerman at the Jet Propulsion Laboratory; C. Casteneda and T. Ward at the University of California, Davis; M. G. McHarg and D. Dunlap at the United States Air Force Academy; and D. Arnfield, Utah State University.

REFERENCES

[1] Purvis, C. K., Garrett, H. B., Whittlesey, A. C., Stevens, N. J., "Design Guidelines for Assessing and Controlling Spacecraft Charging Effects," NASA Technical Paper 2361, National Aeronautics and Space Administration, 1984.

[2] Lai, S. T., "A Survey of Spacecraft Charging Events," AIAA 1998-1042, *Proceedings of the AIAA 36th Aerospace Sciences Meeting*, Reno, Nevada, 1998.

[3] Vampola, A. L., "The Hazardous Space Particle Environment," IEEE Transactions on Plasma Science, Vol 28, No. 6, 2000, pp. 1831-1839.

[4] Akishin, I., Dunaev, N. M., and Tyutrin, Yu. I., "Model of Radiation Electrification of Dielectrics in Simulating the Effects of Protons in Space," Physics and Chemistry of Materials Treatment, Vol. 25. No. 4, 1991, pp. 380-382.

[5] Akishin, I., Bitoshkin, E. A., Zakharov, N. I., and Tsepyaev. L. I., "Electric Discharge Mechanism of Failure of Solid Dielectrics under Proton Radiation," Physics and Chemistry of Materials Treatment, Vol. 30 No. 3, 1996, pp. 197-199.

[6] Akishin, I., "Electric Discharge Phenomena in Irradiated Dielectrics May Reduce the Reliability of Space and Thermonuclear Equipment," Physics and Chemistry of Materials Treatment, Vol. 31, No. 5, 1997, pp. 457-463.

[7] Khorasanov, G. L., and Rodionov, B. N., "Electric Discharges in Dielectrics Irradiated by Fast Protons," in the Proceedings of the Sixth International Symposium of Materials in a Space Environment, European Space Research and Technology Centre, Noordwijk, The Netherlands, 1994, pp. 413-415.

[8] Gromov, V. V., Sessler, G., and Dersam, R., "Effect of Proton Irradiation on Formation of an Electrical Charge in Polyethylene Terephtalate and Teflon Films," Physics and Chemistry of Materials Treatment, Vol. 26, No. 3, 1992, pp. 255-257.

[9] Boev, S. G. and Paderin, V. A., "Charge Accumulation in Dielectrics Irradiated by Protons," Soviet Physics Journal, Vol. 30 No. 5, 1987, pp. 425-429.

[10] Boev, S. G., Paderin, V.A., and Tyutnev, A. P., "Bulk Charging of Dielectrics by Irradiation with Charged Particles," Journal of Electrostatics, Vol. 26, 1991, pp. 133-142.

[11] Feynman, J., Sitale, G., and Wang, J., "Interplanetary Proton Fluence Model: JPL 1991," Journal of Geophysical Research, Vol. 98 No. A8, 1993, pp. 13,281-13,294.

[12] Feynman, J., Ruzmaikin, A., and Berdichevsky, V., "The JPL proton fluence model: an update," Journal of Atmospheric and Solar-Terrestrial Physics, 64, 2002, pp. 1679-1686.

[13] Dennison, J. R., Frederickson, A. R., Green, N. W., Benson, C. E., Brunson, J., and Swaminanthan, P., "Materials Database of Resistivities of Spacecraft Materials," NASA Space Environments and Effects Program, Contract No. NAS8-02031, "Measurement of Charge Storage Decay Time and Resistivity of Spacecraft Insulators," 739 pages, In Press. To be published electronically by NASA Space Environments and Effects Program as part of the *Charge Collector Knowledgebase 3rd Ed*. at http://see.msfc.nasa.gov/

[14] Dennison, J. R., Abbott, J., Hoffmann, R., Sim, A., Thomson, C. D., and Corbridge, J., *Materials Reports*, NASA Space Environments and Effects Program, "Electronic Properties of Materials with Application to Spacecraft Charging," October 2005. To be published electronically by NASA Space Environments and Effects Program as part of the *Charge Collector Knowledgebase 3rd Ed*. at http://see.msfc.nasa.gov/

[15] Baragiola, R.A., Alonso, E.V., and Florio, A.O., "Electron emission from clean metal surfaces induced by low-energy ions," *Phys. Rev. B*, **19**(1), 121-129 (1979). [H^+]

[16] Berger, M.J., Coursey, J. S., Zucker, M. A., Chang, J., "Stopping-Power and Range Tables for Electrons, Protons, and Helium Ions," National Institute of Standards and Technology, Physical Reference Data, NISTIR 4999, August 2005, http://physics.nist.gov/PhysRefData/Star/Text/contents.html.

[17] Dennison, J. R., Gillespie, J., Hodges, J., Hoffmann, R. C., Abbott, J., Hunt, A. W., and Spalding, R., "Radiation Induced Conductivity of Highly-Insulating Spacecraft Materials," *Proceedings of the 10th Spacecraft Charging and Technology Conference, (*Biarritz, France, June 18-21, 2007).

[18] Frederickson, A. R. and Dennison, J. R., "Measurement of Conductivity and Charge Storage in Insulators Related to Spacecraft Charging," IEEE Transactions on Nuclear Science, Vol. 50 No., 6, December 2003, pp. 2284-2291.

[19] Green, N. W., Frederickson, A. R., and Dennison, J. R., "Experimentally Derived Resistivity for Dielectric Samples from the CRRES Internal Discharge Monitor," IEEE Transactions on Plasma Science, Vol. 34, No. 5, October 2006, pp. 1973-1978.

[20] Dennison, J. R., Brunson, J., Swaminathan, P., Green, N. W., and Frederickson, A. R., "Methods for High Resistivity Measurements Related to Spacecraft Charging," IEEE Transactions on Plasma Science, Vol. 34, No. 5, October 2006, pp. 2191-2203.

[21] Cazaux, J., "Some considerations on the secondary electron emission δ, form e^- irradiated insulators," J. Appl. Phys. 85 (2), 1137-1147 (1999).

[22] Cazaux, J., "A new model of dependence: secondary electron emission yield on primary electron energy for application to polymers", *J. Phys. D: Appl. Phys.*, **38**, 2005, pp. 2433-2441.

[23] Meyza, X., Goeuriot, D., Guerret-Piecout, C., Treheux, D., Fitting, H.-J., "Secondary Electron Emission and Selfconsistent Charge Transport and Storage in Bulk Insulators: Application to Alumina," J. Appl. Phys., vol. 94, pp. 5384- 5392, 2003.

[24] Thomson, C., "Measurements of the Secondary Electron Emission Properties of Insulators," PhD Dissertation, Utah State University, Logan, UT, USA, March 2004.

[25] Bethe, H. A., "Theory of passage of particles through matter," Ann. Physik,' vol. 5, p. 325 (1930)

[26] Rathi, S. K., Sehgal, M. L., "Ranges of electrons," Journal of Physics, D: Applied Physics, Vol. 8, 1975, pp. 1480-1486.

[27] Reimer, L. *Scanning Electron Microscopy*, (Springer-Verlag, Berlin, 1985).

[28] JR Dennison, R.C. Hoffmann, and J. Abbott, "Triggering Threshold Spacecraft Charging with Changes in Electron Emission from Materials," AIAA-2007-1098, *Proceedings of the 45th AIAA Aerospace Sciences Meeting*, 16 pages, Reno, NV, January 10, 2007.

[29] Fowler, J. F., "X-Ray Induced Conductivity in Insulating Materials", *Proceedings of the Royal Society of London. Series A, Mathematical and Physical Sciences*, Vol. 236, No. 1207 (1956